# Three-dimensional (3D) moment imaging with a USB3 oscilloscope

Yasashri Ranathunga<sup>1</sup>, Temitayo Olowolafe<sup>1</sup>, Suk Kyoung Lee<sup>1</sup> and Wen Li<sup>1, a)</sup>

<sup>1</sup>Department of Chemistry, Wayne State University, Detroit, Michigan, 48202, USA

a) Corresponding author: wli@chem.wayne.edu

Abstract: We report a new implementation of a recently developed 3D momentum imaging technique [Lee et al JCP, 141, 220121 (2014)]. The previously employed high-speed digitizer in the setup is replaced by a portable USB3 oscilloscope. A new triggering scheme was developed to suppress trigger jitters and to synchronize the signals from a camera and the oscilloscope. The performance of the setup was characterized in the study of laser desorption/ionization of 2,5-dihydroxybenzoic acid (DHB) on a velocity map imaging apparatus. A ~60 picosecond time resolution in measuring time-of-flight (ToF) is achieved with a count rate of ~ 1 kHz, comparable to the system using high-speed digitizers. The new setup affords great portability and a wider accessibility to the high-performing 3D momentum imaging technique.

### **I.INTRODUCTION**

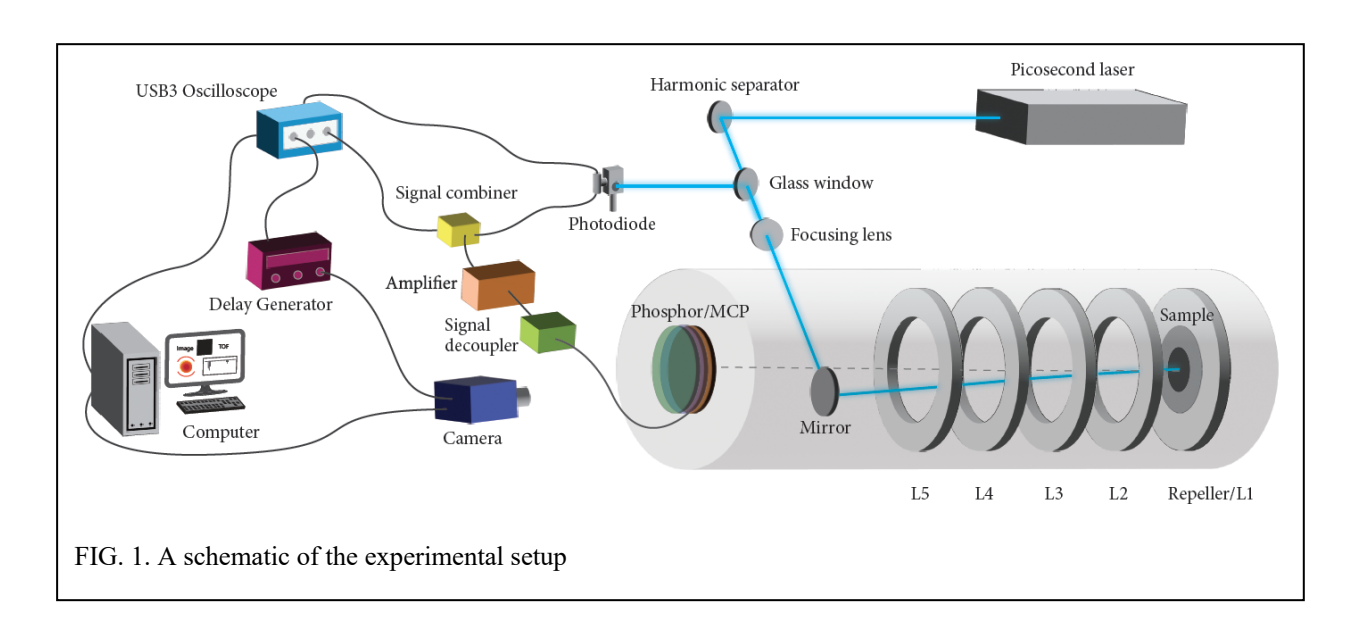
Position- and time-sensitive detectors (3D) are widely employed in many research fields to measure the nascent three-dimensional momentum vectors of charged particles, which are then used to elucidate the dynamical processes that produce the particles. Many types of 3D detectors have been developed over the years and they include delay line detectors<sup>1-4</sup>, cross wire detectors<sup>5</sup>, wedge-strip detectors<sup>6, 7</sup>, dual-CCD detectors<sup>8</sup>, and pixelated semiconductor detector<sup>9-13</sup>. Recently, Li and coworkers introduced a 3D momentum imaging technique employing a low-cost fast frame camera (1 kHz) and a high-speed digitizer, in addition to a standard microchannel plates (MCPs)/phosphor screen 2D imaging detector<sup>14-19</sup>. In this system, the positions of the particles are obtained using a camera while the time-of-flight of the same particles are obtained by digitizing and timing electric signals associated with particle hits on the MCPs using a high-speed waveform digitizer. The system has achieved great performance in terms of time resolution and reduction of dead time when detecting multiple particles. The multi-hit capability is achieved by correlating the brightness of the electron/ion spots from the camera and the height of the ToF peaks from the digitizer.

The adoption of the high-speed digitizer in the setup is critical for achieving great time resolution and multi-hit capability. The fully digitized waveforms enable a sub-sampling resolution in measuring the time of flight of particles. For electrons, typically employed digitizers have a sampling rate of 5 Giga samples/second (GS/s), corresponding to a sampling period of 200 ps. With the oversampling condition, properly suppressed trigger jitter, and an efficient peak

detection algorithm, it has been shown that a ToF resolution of ~30 picoseconds can be achieved <sup>15</sup>. On the other hand, one technical question remains on whether oscilloscopes can achieve the same goal in this setup. After all, digital oscilloscopes execute the same function as a digitizer, *i. e.* digitizing fast electric signals. However, compared to a dedicated high-speed digitizer, which often requires a desktop PC or a dedicated PXI system to function, an oscilloscope has similar or faster sampling rates but with much better accessibility and portability. Previously, these were ruled out because they have a limited transfer bandwidth (1 Megabytes/sec, typical) to a host PC, on which the peak detection algorithm is implemented. The transfer speed is crucial for achieving fast data acquisition, especially when high repetition rate lasers (1 kHz) are employed. More recently, USB-based oscilloscopes start to blur the boundary between oscilloscopes and high-speed digitizers by achieving a significant speed bump in transfer rate (100MB/sec) while still maintaining their great accessibility and portability. Here in this work, we show that it has become possible to adopt a USB oscilloscope in the WSU 3D momentum imaging setup. With careful design and implementation of a new triggering scheme, the setup can achieve great performance with a decent data acquisition rate at 1 kHz, which is sufficient for many existing momentum imaging setups employing lasers running at 1 kHz. We demonstrate the performance of the modified system using laser desorption ionization from organic materials and show the time resolution is high enough to catch the space charging process on repeatedly irradiated sample surfaces.

## **II.EXPERIMENTAL METHODS**

The overall experimental setup is shown in Fig 1. The newly built vacuum chamber features a 5-lens velocity map imaging (VMI) spectrometer with a total ToF length of 24 cm (10 cm lens stack length plus 14 cm field free



length). All the electrodes were made of 2 mm thick 304 stainless steel having a 5-inch outer diameter (OD) and 3-inch inner diameter (ID). The laser system is a 1kHz Nd: YAG picosecond laser (Photonics Industries, RX-355-MWB), which outputs a combined 200  $\mu$ J/pulse energy of the fundamental (1064 nm), the second harmonic (532nm) and the third harmonic (355 nm). After two harmonic separators, ~ 100  $\mu$ J/pulse of the 355 nm light is obtained. A variable neutral density (ND) filter (Thorlabs) is used to adjust the power sent to the VMI chamber for experiments. A reflection geometry approach using a focusing lens (f = 400 mm) outside of the chamber and a flat mirror (at a 45-degree angle) inside the chamber is employed to introduce a focused laser beam to the surface of the substrate. The flat mirror is installed off-center so that it does not block the flying path of the ions and electrons.

The 3D imaging system comprises three major components: a conventional MCP/phosphor screen imaging detector (Photonis APD with 75 mm dia. dual MCPs and P47 phosphor), a fast-frame complementary metal-oxide semiconductor (CMOS) camera, and a USB oscilloscope. After the ions/electrons are produced by laser irradiation, they leave the surface and are accelerated and momentum-focused by the VMI spectrometer before impinging on the MCP detector and producing light flashes on the phosphor screen. A USB3 CMOS camera (Basler acA720-520 µm) equipped with a Sony IMX287 sensor is used to register the positions (X, Y) of the particle hits. The camera is run in the external trigger mode and its resolution is set at 260×260 pixels. It can run at 1 kframes/s with superior imaging quality. The USB3 oscilloscope (Picotech 6403D) was used to digitize the electric signal from the MCPs to extract the ToFs of particle hits. 6403D is a 4-channel oscilloscope with a bandwidth of 350 MHz and a maximum sampling rate of 5 GS/s (one channel), which corresponds to a 200 ps sampling period.

A structural difference between an oscilloscope and a digitizer and its consequence need to be addressed and this issue makes the task of replacing the digitizers with oscilloscopes non-trivial. While the analog-to-digital (ADC) circuitry is similar between an oscilloscope and a digitizer, a significant difference is present in the structure and function of the on-board memory, which is used to store the digitized waveforms before they are transferred to a host PC. To facilitate a fast data transfer, a digitizer implements a first-in-first-out (FIFO) queue structure, with which the acquisition and transfer can take place simultaneously. However, in oscilloscopes, the data transfer is initiated only after all the requested data points are acquired by the ADC circuitry. Even though the transfer speed has increased significantly for oscilloscopes, a time gap is present due to the single-port memory structure. This reduces the duty cycle of data acquisition to less than 100% (in our case, we achieved a ~96% duty cycle). Increasing the transfer speed

will reduce the time gap but will not completely remove it. This poses some challenges in synchronizing the data from the camera and those from the oscilloscope. Previously, both the digitizer and the camera are triggered by the laser at its full repetition rate (1 kHz), and it is relatively easy to synchronize. Timestamps can be used to achieve synchronization<sup>12</sup>. However, oscilloscopes often do not come with a hardware timestamp function and software timestamps are not accurate enough. Furthermore, oscilloscopes lack trigger jitter interpolators (a time-to-digital (TDC) circuitry to measure accurate trigger time), which can be used to suppress the jitter associated with starting triggering point. This is critical to achieving a sub-sampling resolution. A different approach is needed. In this study, we develop a new triggering scheme to synchronize the camera with the digitizer as well as to suppress the jitters. The scheme is shown in Fig. 1 and can be summarized in the following step: (1) The oscilloscope is triggered by the laser signal picked off by a photodiode on the external trigger input (AUX port is configured to accept external trigger). This signal serves as a starting point for data acquisition; (2) The laser signal from the photodiode is also combined with the MCP signal (after amplification using an Ortec FTA 420 fast amplifier) with a signal combiner (Mini-circuits ZAPD-1+) and the combined signal is then sent to the channel 1 of the oscilloscope to be digitized. The MCP signal is picked off using a conventional capacitive coupling scheme with a 2.2 nF capacitor (signal decoupler in Fig. 1). Distortions of the MCP signals due to ringing in the circuit do exist in the digitized waveforms but they do not appear to significantly impact the ToF performance. The presence of both the laser signal and the MCP signal in the same waveform allows direct extraction of ToFs regardless of the trigger jitter. A similar approach was adopted previously but it was employed to increase the system count rate<sup>12</sup>; (3) Using the built-in waveform generator, the oscilloscope outputs a TTL signal on its OUTPUT port whenever an acquisition is triggered. This signal is sent to trigger a delay generator (BNC, model 555), which in turn triggers the camera. During the data transfer process, even though the laser is still firing, neither the oscilloscope nor the camera is taking data. In this way, the camera frames are now synchronized with the oscilloscope waveforms. Depending on the speed of the host computer, the duty cycle can reach as high as 96% at 1 kHz, which means the effect acquisition rate is 960 Hz. The duty cycle improves to 100% with a lower repetition rate but will drop if the repetition rate goes higher than 1 kHz. A typical length of waveforms is 1000 data points, corresponding to a record length of 200 ns. We should note the 6403D oscilloscope has a large memory capacity of 1 GS and a small trigger re-arm time (a few microseconds). This means if real-time data display is not needed and total data points are within 1 GS, the oscilloscope will be able to achieve 100% duty cycle at a much higher rate (>100 kHz) because it does not have to transfer the data until the end of the acquisition and thus avoids

timing overhead. It seems these two features (a large memory and a short re-arm time) are quite universal among oscilloscopes on the market and suggests this mode of operation (one acquisition plus one transfer) can be applied to many other oscilloscopes.

The computer used in data acquisition is a regular Windows 10 desktop featuring an AMD 5600G central processing unit (CPU) processor and 16 GB memory, which is a typical configuration for a low to mid-range performance desktop. This suggests that the 96% duty cycle achieved here does not require special computing equipment. A faster-clocked computer might further help with the speed and thus the duty cycle but remain unexplored. A Labview program was written to integrate the data acquisition from both the camera and the oscilloscope.

It should be also noted the delay generator is optional because the delay needed to match the camera exposure and particle hits can be provided using the built-in signal generator. It is employed here because we plan to run two cameras in the future, which are triggered at different exposure delays to capture both electrons and ions<sup>20</sup>.

#### **III.RESULTS AND DISCUSSIONS**

We first use photon hits to characterize the time resolution of the ToF detection scheme. This is done by using some light reflected from the surface which happens to hit the detector. Here the voltages on the VMI lens are turned

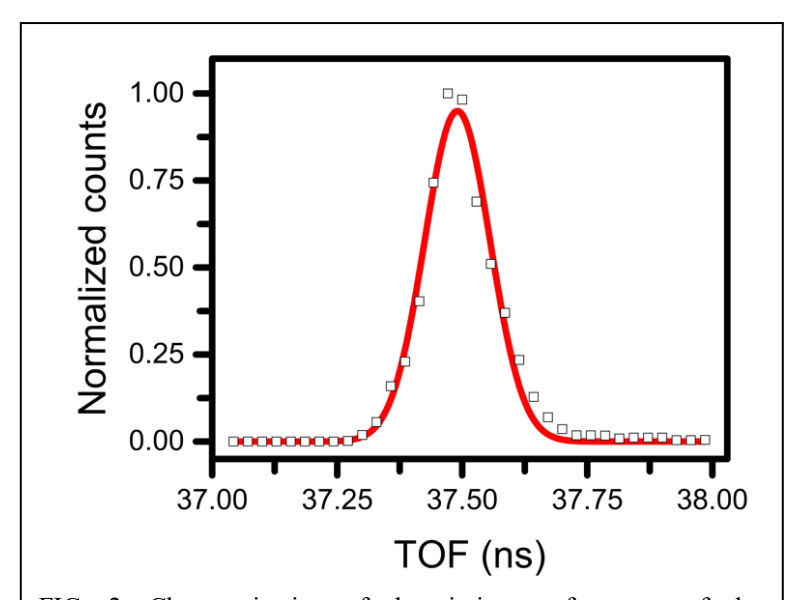


FIG. 2. Characterization of the timing performance of the oscilloscope-based 3D VMI method using short laser pulses (10 ps). The red curve is a Gaussian fitting to the experimental data (square). The FWHM of the curve is 0.15 ns.

off so neither ions nor electrons can reach the detector. Because of the short pulse duration of the laser (10 ps), the photon hit provides a good system to measure the time resolution of the system. In each digitized waveform, the difference between the position of the peak corresponding to the photon hit and that of the laser signal from the photodiode is taken as the ToF of the photon arrival. This scheme suppresses trigger jitters and is critical for achieving a good ToF resolution. Fig. 2 shows the

time-of-flight distribution of the photon signal fitted to a Gaussian function. The full-width half maximum (FWHM) of the fitting is 0.15 ns, which corresponds to a time resolution of  $\sim 64$  ps (standard deviation). The value is lower than previously achieved with a high-speed digitizer, possibly due to the quality of the ADC circuitry of the oscilloscope. Nonetheless, this resolution is high enough to perform 3D electron/ion momentum imaging.

To test the real-world performance of the new setup, we detected photoelectrons arising from surface photoemission of 2,5-Dihydroxybenzoic acid, a common matrix used in matrix-assisted laser desorption/ionization (MALDI). While MALDI is a popular analytical tool for ionizing biological samples, the initial ionization dynamics of the matrix are poorly understood<sup>21</sup>. Our apparatus was built to study this process. The thin film sample (99%, Sigma-Aldrich) was prepared using vacuum sublimation on a stainless-steel disc substrate. The substrate was then placed on a threaded stainless steel ring and secured using copper conductive tape. The stainless-steel ring was mounted onto the first electrode (Repeller) in the VMI apparatus with the film facing the laser beam and the detector.

The experiment was done by continuously irradiating the surface for 15 minutes with a laser power of 2 µJ/pulse and two data sets (Fig. 3A, D and B, E) on ejected electrons were collected for 5 minutes each during this time. Only

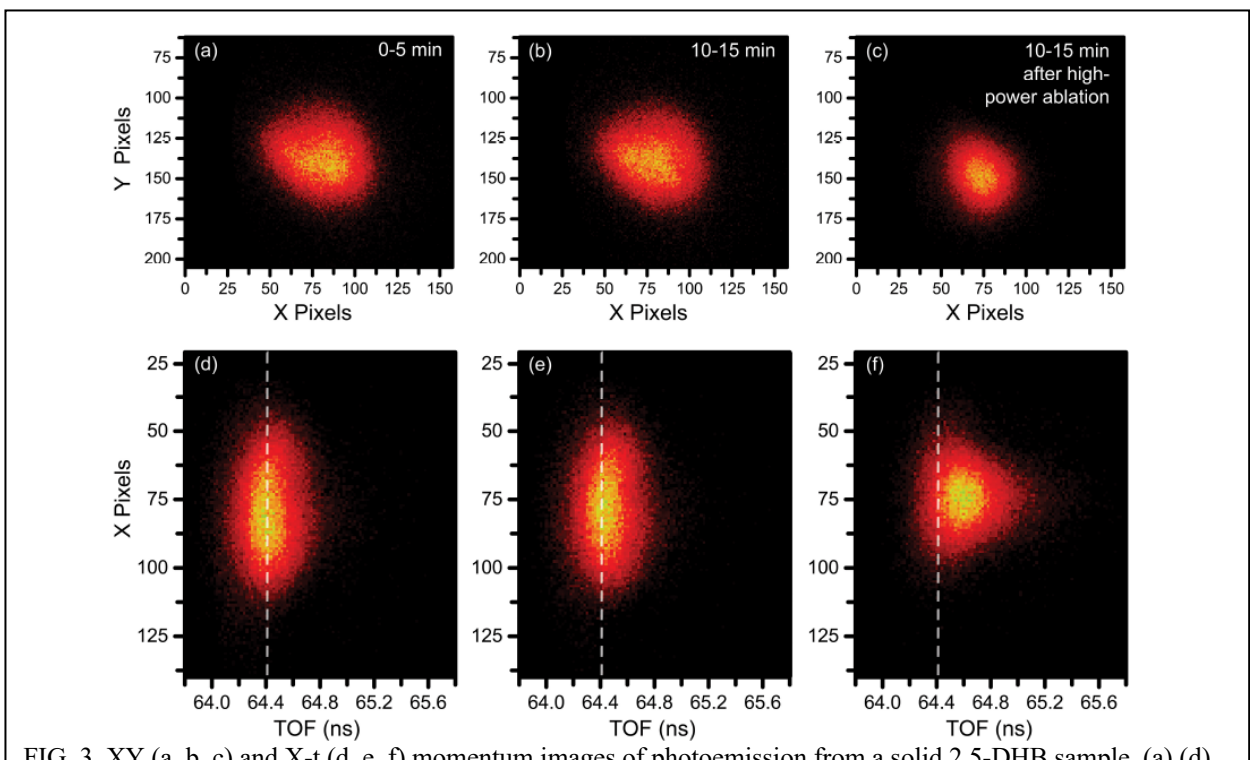


FIG. 3. XY (a, b, c) and X-t (d, e, f) momentum images of photoemission from a solid 2,5-DHB sample. (a) (d) are for photoelectrons produced in the first 5 minutes; (b)(e) are for photoelectrons produced between 10 to 15 minutes after 1 min. of high-power laser irradiation (70  $\mu$ J/pulse). All data were taken at a laser power of 2  $\mu$ J/pulse. During the high-power irradiation, the voltages on the detector and the VMI electrodes were all turned down to protect the detector.

photoemission took place at this power because the power is below the MALDI threshold, and no ions were detected. The electron count rate is about 0.4/pulse. Then the laser power was increased to (70 µJ/pulse) and the surface was irradiated at this power for 1 minute. At this power, sample loss due to MALDI is expected. After the high-power irradiation, the laser power was restored to 2 µJ/pulse right away and one more 5-minute-long data was taken starting at 10 minutes (Fig. 3C, F). Fig. 3 shows the XY and X-t momentum distributions of the ejected photoelectrons (X, Y are the spatial coordinates of electron hits on the detector and t is the ToF). In Fig. 3D, the peak of the time-of-flight distribution is at 64.40 ns, marked as the white dashed line (also shown in Fig 3E and F as a reference). Fig. 3E shows the peak of ToF has changed to 65.46 ns, 60 ps longer than that at the first five minutes. Because all the experimental conditions remain the same, we hypothesize the slight shift of ToF is due to positive charge build-up on the surface as electrons are continuously removed under laser irradiation. 2,5-DHB is an insulator and negative charges cannot be quickly replenished from the metal substrate and the electrode. We estimate about 300,000 electrons were removed during the overall 10 minutes of irradiation and this has a small but discernible effect on the electron ToF. This was captured due to the high ToF resolution of the setup. Fig. 3C and F show an even more dramatic change after a short duration of high-power laser ablation. The ToF peak is now shifted by 170 ps and the shape has changed to a cone in the X-t image while the size shrinks in the XY image, suggesting an extensive interaction between ejected electrons and a significant amount of positive charge on the surface. Such a build-up of positive charges on the sample surface has not been reported previously for MALDI and further investigation is needed to assess how important this is to the initial ionization dynamics of the matrix and the overall MALDI process.

To summarize, we have demonstrated a modified 3D momentum imaging technique employing a USB3 oscilloscope. The system achieved  $\sim 60$  ps temporal resolution in measuring ToFs. Because both the oscilloscope and the camera have small size footprints and use USB connections with a PC, the system can be easily deployed with a laptop computer. This affords great portability to the system and provides great accessibility to the high-performing 3D momentum imaging technique. With the high ToF performance and the 3D imaging capability, we were able to observe a subtle but potentially important effect in the MALDI process, which will be studied in more detail in the future.

#### **IV.ACKNOWLEDGMENT**

This material is based upon work supported by the National Science Foundation under Award No. CHE 2107860 (photoemission from surfaces). We would like to thank Chamod Dharmadasa and Prof. Charles Winter for their help in preparing the DHB sample.

#### **V.REFERENCES**

- <sup>1</sup>H. Keller, G. Klingelhöfer and E. Kankeleit Nucl. Instr. Meth. Phys. Res. A **258**, 221 (1987).
- <sup>2</sup>G. Da Costa, F. Vurpillot, A. Bostel, M. Bouet and B. Deconihout Rev. Sci. Instrum. **76**, 013304 (2005).
- <sup>3</sup>K. A. Hanold, A. K. Luong, T. G. Clements and R. E. Continetti Rev. Sci. Instrum. **70**, 2268 (1999).
- <sup>4</sup>O. Jagutzki, A. Cerezo, A. Czasch, R. Dorner, M. Hattas, H. Min, V. Mergel, U. Spillmann, K. Ullmann-Pfleger, T. Weber, H. Schmidt-Bocking and G. D. W. Smith IEEE Trans. Nucl. Sci. **49**, 2477 (2002).
- <sup>5</sup>J. Becker, K. Beckord, U. Werner and H. O. Lutz Nucl. Instr. Meth. Phys. Res. A 337, 409 (1994).
- <sup>6</sup>O. Jagutzki, J. S. Lapington, L. B. C. Worth, U. Spillman, V. Mergel and H. Schmidt-Böcking Nucl. Instr. Meth. Phys. Res. A 477, 256 (2002).
- <sup>7</sup>C. Martin, P. Jelinsky, M. Lampton, R. F. Malina and H. O. Anger Rev. Sci. Instrum. **52**, 1067 (1981).
- <sup>8</sup>D. Strasser, X. Urbain, H. B. Pedersen, N. Altstein, O. Heber, R. Wester, K. G. Bhushan and D. Zajfman Rev. Sci. Instrum. **71**, 3092 (2000).
- <sup>9</sup>A. Nomerotski, M. Brouard, E. Campbell, A. Clark, J. Crooks, J. Fopma, J. J. John, A. J. Johnsen, C. Slater, R. Turchetta, C. Vallance, E. Wilman and W. H. Yuen J. Instrum. **5,** C07007 (2010).
- <sup>10</sup>A. T. Clark, J. P. Crooks, I. Sedgwick, R. Turchetta, J. W. L. Lee, J. J. John, E. S. Wilman, L. Hill, E. Halford, C. S. Slater, B. Winter, W. H. Yuen, S. H. Gardiner, M. L. Lipciuc, M. Brouard, A. Nomerotski and C. Vallance J. Phys. Chem. A **116**, 10897 (2012).
- <sup>11</sup>A. Zhao, M. v. Beuzekom, B. Bouwens, D. Byelov, I. Chakaberia, C. Cheng, E. Maddox, A. Nomerotski, P. Svihra, J. Visser, V. Vrba and T. Weinacht Rev. Sci. Instrum. **88**, 113104 (2017).
- <sup>12</sup>D. A. Debrah, G. A. Stewart, G. Basnayake, A. Nomerotski, P. Svihra, S. K. Lee and W. Li Rev. Sci. Instrum. **91**, 023316 (2020).
- <sup>13</sup>M. Davino, E. McManus, N. G. Helming, C. Cheng, G. Moğol, Z. Rodnova, G. Harrison, K. Watson, T. Weinacht, G. N. Gibson, T. Saule and C. A. Trallero-Herrero Rev. Sci. Instrum. **94**, 013303 (2023).
- <sup>14</sup>S. K. Lee, F. Cudry, Y. F. Lin, S. Lingenfelter, A. H. Winney, L. Fan and W. Li Rev. Sci. Instrum. **85**, 123303 (2014).
- <sup>15</sup>S. K. Lee, Y. F. Lin, S. Lingenfelter, L. Fan, A. H. Winney and W. Li J. Chem. Phys. **141**, 221101 (2014).
- <sup>16</sup>Y. F. Lin, S. K. Lee, P. Adhikari, T. Herath, S. Lingenfelter, A. H. Winney and W. Li Rev. Sci. Instrum. **86**, 096110 (2015).
- <sup>17</sup>Q. Liao, A. H. Winney, S. K. Lee, Y. F. Lin, P. Adhikari and W. Li Phys. Rev. A **96**, 023401 (2017).
- <sup>18</sup>G. Basnayake, Y. Ranathunga, S. K. Lee and W. Li J. Phys. B-At. Mol. Opt. Phys. **55**, 023001 (2022).
- <sup>19</sup>L. Fan, S. K. Lee, P.-Y. Chen and W. Li J. Phys. Chem. Lett. **9**, 1485 (2018).
- <sup>20</sup>L. Fan, S. K. Lee, Y.-J. Tu, B. Mignolet, D. Couch, K. Dorney, Q. Nguyen, L. Wooldridge, M. Murnane, F. Remacle, H. Bernhard Schlegel and W. Li J. Chem. Phys. **147**, 013920 (2017).
- <sup>21</sup>G. A. Stewart, D. Debrah, Y. Ranathunga, T. A. Olowolafe, H. B. Schlegel, S. K. Lee and W. Li J. Phys. Chem. C **126**, 17135 (2022).